journal

Processing Dependence of Texture, and Critical Properties of YBa$_2$Cu$_3$O$_{7-\delta}$ Films on RABiTS Substrates by a Non-Fluorine MOD Method

Y. Xu,[†,‡] A. Goyal, K.J. Leonard, and E.D. Specht

Metals and Ceramics Division, Oak Ridge National Laboratory, Oak Ridge, Tennessee 37831

D. Shi

Department of Materials Science, University of Cincinnati, Cincinnati, Ohio 45221

M. Paranthaman

Chemical Sciences Division, ORNL, Oak Ridge, Tennessee 37831

YBa$_2$Cu$_3$O$_{7-\delta}$ (YBCO or Y123) films on rolling-assisted biaxially textured substrates (RABiTS) were prepared via a fluorine-free metallorganic deposition (MOD) through spin coating, burnout, and high temperature anneal. The effects of substrate texture and surface energy of the CeO$_2$ cap layer were investigated. Except for the commonly accepted key factors, such as the textures of substrate and buffer layers, we found some other factors, for example, the deposition temperature of the cap layer, are also critical to the epitaxial growth of Y123 phase. With the CeO$_2$ cap layer deposited at relative high temperature of 700°C, a critical current density, J_c, over 1 MA/cm^2 has been demonstrated for the first time on Ni-RABiTS by a fluorine-free MOD method. Whereas for samples with CeO$_2$ cap layers deposited at a lower temperature of 600°C, even though XRD data showed a better texture on these buffer layers, texture degradations of YBCO grains under the optimized processing conditions were observed and a lower oxygen partial pressure around 40 ppm was necessary for the epitaxial growth of Y123 phase. As a result, J_c fell to 0.45 MA/cm^2 at 77 K. The observed phenomena points to the change of surface energy and reactivity of the CeO$_2$ cap layer with respect to the CeO$_2$ deposition temperature. In this paper, the YBCO phase diagram was also summarized.

I. Introduction

SOON after the discovery of the cuprate high temperature superconductor (HTS), chemical solution depositions (CSD) were developed to grow YBa$_2$Cu$_3$O$_{7-\delta}$ (YBCO) films.[1–5] Now three major CSD approaches are in use for the ReBCO (Re, rear earth) deposition[6–9]: (1) sol–gel processes that use 2-methoxyethanol as reactant/solvent, (2) hybrid processes that use chelating agents such as acetylacetonates or diethanolamine to reduce alkoxide reactivity, and (3) metal organic decomposition (MOD) techniques that use high-molecular weight precursors and water-insensitive carboxylates, for example 2-ethyl-hexanoates, etc. These CSD routes have been used for growing both oxide buffer layers and HTS films. Whereas the critical current

density, J_c, was usually very low and it was believed that the carbon-contained precursor might have resulted in the formation of stable BaCO$_3$ at grain boundaries.[10] In 1988, Gupta *et al.*[11] reported a new method of using metal trifluoroacetate (TFA) precursors to grow textured YBCO films on single crystal substrates. Mclntyre *et al.*[12] further developed this method and high J_cs over 1 MA/cm^2 had been demonstrated on thin YBCO films. As the stability of BaF$_2$ is greater than that of BaCO$_3$, fluorine can be removed in a humid environment at temperature above 650°C.[13] Hence, the use of TFA salts appears to avoid the formation of barium carbonate. Now, the MOD using TFA is a well-established CSD route for the coated conductor development.[11,14–18] Nevertheless, the interest in the fluorine-free MOD approach remains. The most important being is that the removal of fluorine in the form of HF at the conversion temperature is a non-trivial process. There appear to be many issues related to the fluid-flow and complicated reactor designs. Moreover, the HF release as a byproduct in the TFA approach is a major environmental concern especially for a large-scale production.

YBCO films prepared through the fluorine-free precursor[19] of trimethylacetates in amylamine and propionic acid (TMAP) have shown J_c over 1.6 MA/cm^2 at 77 K on single crystal substrates.[20] In this paper, J_cs over 1 MA/cm^2 at 77 K for 0.2 μm YBCO films have been successfully demonstrated on rolling-assisted biaxially textured substrates (RABiTS).[21] The data in this research show that the fluorine-free TMAP MOD approach is promising for the YBCO coated conductor fabrication. Moreover in this paper, the YBCO phase diagram was summarized.

II. Experimental Procedure

(1) Preparation of Coating Solution

Y(C$_4$H$_9$COO)$_3$ and Cu(C$_4$H$_9$COO)$_2$ were home-made compounds by reacting metal nitrides with ammonium trimethylacetate at room temperature (RT), respectively. All other chemicals were from Alfa Aesar (Ward Hill, MA). Steps of the solution preparation is shown in the flow chart (Fig. 1). Usually the solution's viscosity was adjusted to 30–100 cross polarizations and the oxide contents were around 10–12 wt% with a total ionic concentration of 1.0 ∼1.2 mol/L.[20]

(2) Preparation of Ni and Ni-3W Substrates with Buffer Layers

Architectures of the RABiTS used in this experiment are shown in Fig. 2. Biaxially textured Ni and NiW substrates were prepared through the standard RABiTS process.[9,21,22] The buffer stack of Ni-RABiTS includes a 12 nm CeO$_2$ seed layer, a 300 nm

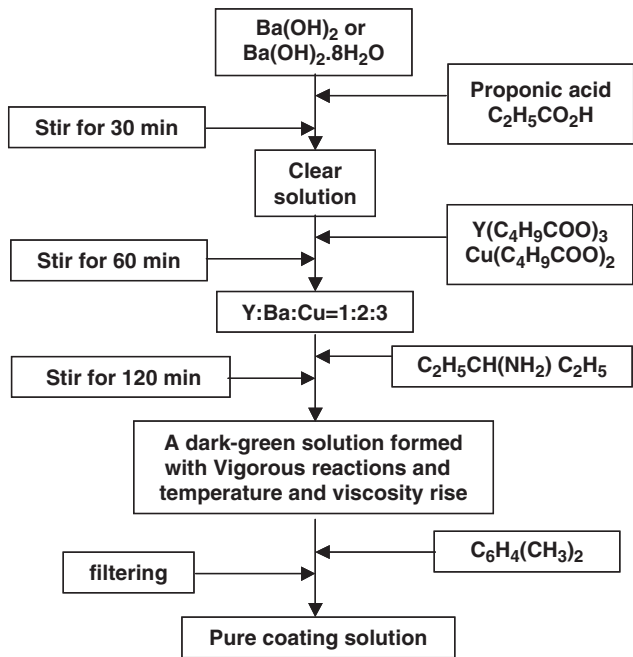R. Bordia—contributing editor

Fig. 1. Flow chart of the solution preparation in the fluorine-free approach of TMAP by using the trimethylacetate precursors and propionic-amine solvent system.

YSZ barrier, and a 20 nm CeO_2 cap. The seed layer was grown by reactive e-beam deposition at 700°C. The barrier and the cap were deposited by radio frequency sputtering at 700°C in 5–10 mTorr forming gas. For NiW–RABiTS, the major difference in the buffer deposition is that the CeO_2 cap was grown at 600°C, 100°C lower than did on Ni-RABiTS.

(3) Coating, Burnout, and High Temperature Anneal

Precursor films were prepared by spin coating at 2000 rpm for 30 s at ambient temperature and pressure. The as-coated film, green film, of about 2 μm were condensed to 0.2 μm through burnout and high temperature anneal. All samples were burnout at the same conditions as reported previously.[20] After high temperature conversion, silver contacts around 1 μm in thickness were sputtered onto YBCO films at RT. The oxygen anneal was performed at 500°C for 1 h followed by a cooling ramp of 2°C/min to 350°C to diffuse oxygen into the YBCO perovskite structure and to establish good contact of Ag with YBCO films.

(4) Characterization

Critical transition temperature, T_c, and critical current, I_c, were measured with the direct four-probe transport method. The criterion for the I_c measurement is 1 μV/cm and J_c is calculated based on I_c value and the cross-sectional area of YBCO films. X-ray diffractions (XRD) of the θ–2θ scan (A Philips XRG3100 diffractometer with CuK$_\alpha$ radiation) were used for the phase examination. ω-scans, φ-scans, and pole-figures were performed on four-circle diffractometer (diffractometer 3488M-401 with CuK$_\alpha$ radiation, $\lambda = 1.54$ Å) to characterize in-plane and out-of-plane textures. We use volume fraction of cubic phase (VFCP) as one of the reference criterion for the texture characterization, which is defined as follows: we collect one pole figure (note: the pole figure was collected on (111) plane for NiW, YSZ, and CeO_2; on (222) plane for Y_2O_3, and on (113) plane for YBCO) and one background pole figure, offset in 2θ. We take the difference. Because the background pole figure may contain reflections from other phases, giving spurious negative values in the difference pole figure. We set all negative values to zero, then normalize the pole figure. Most often we see only a single (twinned) (001) ⟨100⟩ orientation, giving four peaks with only noise at other directions. We integrate the cube peaks and express this as a fraction of the total intensity. For example,

a volume fraction of 90% says that we see only one orientation, but concedes that other more weakly textured orientations may be present at ∼10% volume fraction. Surface morphology was observed by scanning electron microscopy (SEM). The cross-sectional interface structure was examined with transmission electron microscopy (TEM) and selected area diffraction (SAD). Thickness and stoichiometry were determined by Rutherford backscattering spectroscopy (RBS) with 5 MeV He^{2+} ions near normal incidence and detected at 160° scattering angle. By using RBS, the thickness could be measured down to 0.5−1 nm, and errors for the composition measurement should be within 5%.

III. Experimental Results and Discussions

Texture data in transverse direction of RABiTS and buffer layers are listed in Table I. Usually, peaks in the rolling direction are sharper and the full-width at half-maximum (FWHM) values are 1°–2° smaller than those in the transverse direction. In plane and out-of-plane texture, and especially VFCP of RABiTS and buffers, are the key factors that affect YBCO alignment.[23] The FWHM in the rocking curve (Δω) of CeO_2 cap layer on NiW–RABiTS is about 3°–3.5° smaller than that on Ni–RABiTS. Although the broader rocking curve may be from the added combination of the seed and the cap layers on Ni–RABiTS, the fact that the value of VFCP is 5.9% smaller than that on NiW–RABiTS indicates the inferior texture of the CeO_2 cap layer on Ni–RABiTS compared with those on NiW–RABiTS.

In addition to the texture effect, the deposition conditions of the cap layer, such as the deposition temperature, should be considered as well. Because the activity of the cap layer is a control factor for the nucleation and growth of Y123 phase in terms of barrier energy and reactivity. Table II shows typical results of YBCO films deposited on Ni–RABiTS and NiW–RABiTS under different conditions. RBS analysis shows that the composition as well as the film thickness are comparable for those samples prepared under the similar conditions. Figure 3 is a typical RBS spectrum on sample N-180. Apparently, RBS data shows no observable macroscopic compositional difference from the stoichiometry of the solution. Thickness data in RBS analysis agree well with that in cross-sectional TEM observations. The processing conditions used for samples listed in Table II are based on a large number of experiments.[24,25] Under optimized conditions (745°C, 30 min, D.P. = 45°C, and pO_2 = 180 ppm), YBCO films had shown a J_c over 1.6 MA/cm^2 on LAO substrate,[20] and in this work, a J_c of 1.02 MA/cm^2 (sample N-180) has been demonstrated on RABiTS. Nevertheless, under the same processing condition, YBCO films on NiW–RABiTS show no J_c (sample NW-180). Only when partial pressure of oxygen (pO_2) was reduced to a low level of, in this case, 40 ppm (sample NW-40) a J_c of 0.45 MA/cm^2 was shown on NiW–RABiTS. It is well know that once the pO_2 approaches to the unstable line in the YBCO phase diagram, the driving force of YBCO formation is greatly reduced and the growth of Y123 phase slows down or even stops on the regular base as shown on sample N-40. Hence, the results in this group of experiments indicate that the texture of buffer layers is not the only decisive
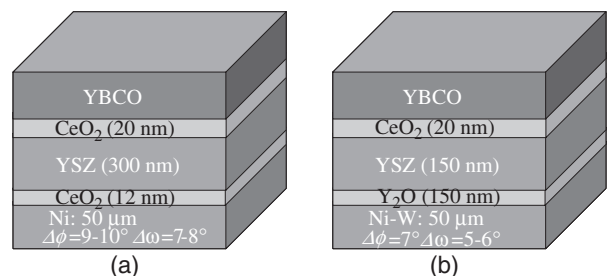
Fig. 2. Architectures of RABiTS with buffers, (a) Ni–RABiTS with CeO_2/YSZ/CeO_2 stack, and (b) Ni-3% W-1.7% Fe (NiW) RABiTS with Y_2O_3/YSZ/CeO_2 stack.

Table I. Texture Data for Architecture NIW/Y₂O₃/YSZ/CeO₂ and Ni/CeO₂/YSZ/CeO₂

Architecture Layers	NiW/Y₂O₃/YSZ/CeO₂				Ni/CeO₂/YSZ/CeO₂		
	NiW	Y₂O₃	YSZ	CeO₂	Ni	CeO₂	YSZ
$\Delta\omega$ (°)	8.2	8.0	6.9	6.8	10.1	10.3	9.1
$\Delta\phi$ (°)	8.0	7.7	8.3	7.7	10.5	10.7	10.2
VFCP (%)	95.2	82.2	97.5	86.1	95.4	80.2	93.9

For Y₂O₃, $\Delta\omega$ was collected from (004) plane and $\Delta\phi$ from (222), but for NiW, YSZ, and CeO₂ the $\Delta\omega$ values were from (002) planes and $\Delta\phi$s from (111).

factor for high quality YBCO growth, other factors had played roles either. To make a better understanding, ω-scan and ϕ-scan were performed on these samples. For Ni-RABiTS with higher CeO₂ deposition temperature of 700°C, when converted at lower pO_2 (40 ppm) intensities in both rocking curve and ϕ-scan drop about 25% compared with samples that processed in $pO_2 = 180$ ppm (Fig. 4). In addition, $\Delta\omega$ increased 1.5° and the VFCP decreased 8.6% as well. T_c has very small drop of about 0.6 K. However, J_c drops more than 88%. The rapid loss in J_c may result either from the reduction in the VFCP or the degradation in texture.

On the other hand, for NiW–RABiTS with a lower CeO₂ deposition temperature of 600°C, better texture was shown for YBCO films processed at $pO_2 = 40$ ppm while YBCO films converted at $pO_2 = 180$ ppm showed very broad FWHM. Figures 5 and 6 are the ω-scan and ϕ-scan showing the out-of-plane and in-plane texture of YBCO films on NW-40 and NW-180, respectively. These results indicate that Y123 phase has not very well nucleated on the CeO₂ cap layer especially for the conversion in a relatively higher pO_2 of 180 ppm. To further investigate the texture, the pole figure analysis was performed on sample NW-180 and N-180 (Fig. 7). Compared with sample N-180, YBCO films on NW-180 showed poor texture with large amount random oriented grains. Obviously, these polycrystalline grains were not formed by interface nucleation, but they may have originated from nuclei that initiated from second phase or other defects in the precursor film. The data in Table II show that, for sample NW-180, the value of VFCP is only 52.5%, which means almost half of YBCO grains were misoriented. In this instance, weak links exist at large angle grain boundaries and superconducting networks are frustrated.

Based on previous reports[26,27] and our experiments,[24] the YBCO phase diagram is summarized in Fig. 8. To avoid the nucleation of *a*-axis oriented grains, a conversion under the condition close to the c2 line or between c1 and c2 lines in the YBCO phase diagram is suggested. For YBCO on RABiTS, a lower conversion temperature has the advantage of reducing substrate oxidation and eliminating delaminations.

With the CeO₂ cap layer prepared at higher temperature, samples converted at low pO_2 of 40 ppm (N-40) do show degradations on texture and electrical properties compared with those converted at $pO_2 = 180$ ppm. As the conversion condition of $pO_2 = 40$ ppm at 745°C approaches the YBCO unstable line in the phase diagram, the driving force of the YBCO formation gets smaller. Accordingly, the epitaxial growth cannot be completed. As a result, the value of VFCP reduces, while $\Delta\omega$ and $\Delta\phi$ may stay the same (see Table II) because of the existence of well-textured bottom layer.

Nevertheless, textures and electric properties were improved when converted at $pO_2 = 40$ ppm on those samples with the cap layer deposited at a low temperature of 600°C (NW series). This result is not in accordance with the trend predicted by the phase diagram. Some other factors may play a role or even dominate in the process. Things that could change the track of YBCO formation include the precursor solution, processing condition, and the interface characteristics. In this set of experiments the solution is the same and the processing conditions are comparable. As many factors have been explored with large amount of experiments and all of the results point to the surface characteristic of CeO₂ cap layer in terms of surface energy and reactivity. Apparently, the deposition temperature of CeO₂ cap affects the free energy. It is reasonable to believe this is the key factor that controls the behavior of YBCO nucleation and growth. We found that lower deposition temperature of CeO₂ cap layer increases the interface reactivity. As shown in Fig. 9(a), a continuous layer of BaCeO₃ was formed between YBCO and CeO₂ for the cap layer deposited at 600°C. With the CeO₂ deposited at high temperature, a clean interface between YBCO and CeO₂ is usually observed by the cross-sectional high resolution TEM, indicating that the formation of the BaCeO₃ was very limited.[25]

The data of specific energy barrier are unavailable, but the trend is clear that the interface energy of YBCO and CeO₂ rises with the increase of the deposition temperature. That is, the higher the deposition temperature the higher the energy barrier, and vice versa. So the size of the critical nuclei of YBCO phase
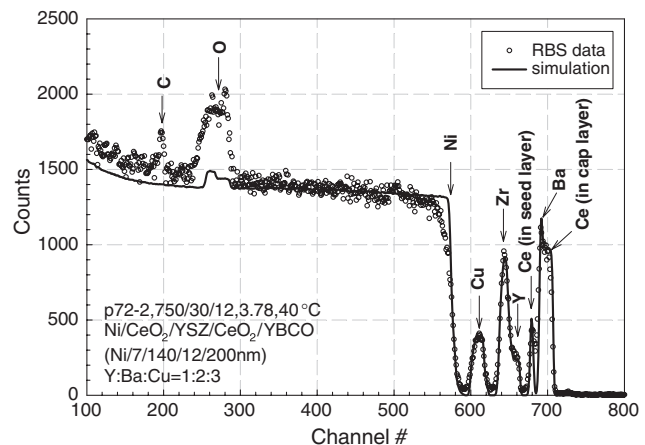

Fig. 3. RBS spectra of sample N-180, showing the results of compositional and thickness analysis. The unfilled circles are measured values and solid line is the simulation. The RBS measurement was performed at 5 MeV He⁺⁺ with backscatter angle of 160°.

Table II. Texture Data and Electrical Properties of YBCO Films Converted in Different Conditions

Sample I.D.	Annealing condition (ppm)	$\Delta\omega$ (°)	I_ω (Counts)	$\Delta\phi$ (°)	I_ϕ (Counts)	VFCP (%)	T_c (°C)	J_c ($\times 10^5$ A/cm²)
N-180	Ni, 180	11.5	1830	10.2	2110	78.2	89.6	10.2
N-40	Ni, 40	13.0	1521	10.1	1345	69.6	89.0	1.2
NW-180	Ni3W, 180	13.5	649	7.2	454	52.5	65.5	0
NW-40	Ni3W, 40	6.5	1867	7.4	1692	64.3	88.8	4.5

The $\Delta\omega$ and $\Delta\phi$ were collected from YBCO (003) and (113) planes, respectively. Pole figure was performed on YBCO (113) plane. VFCP, volume fraction of cubic phase.
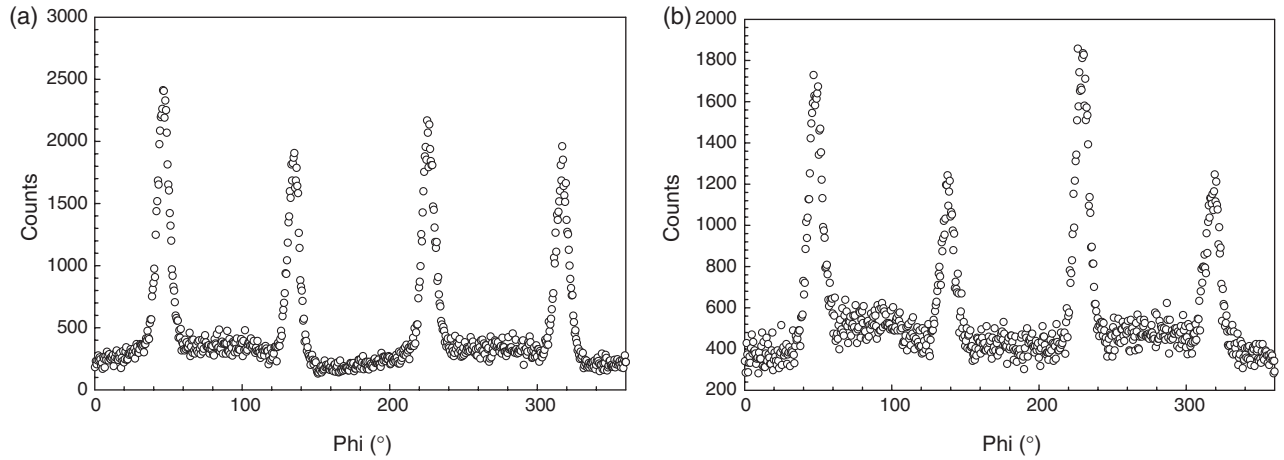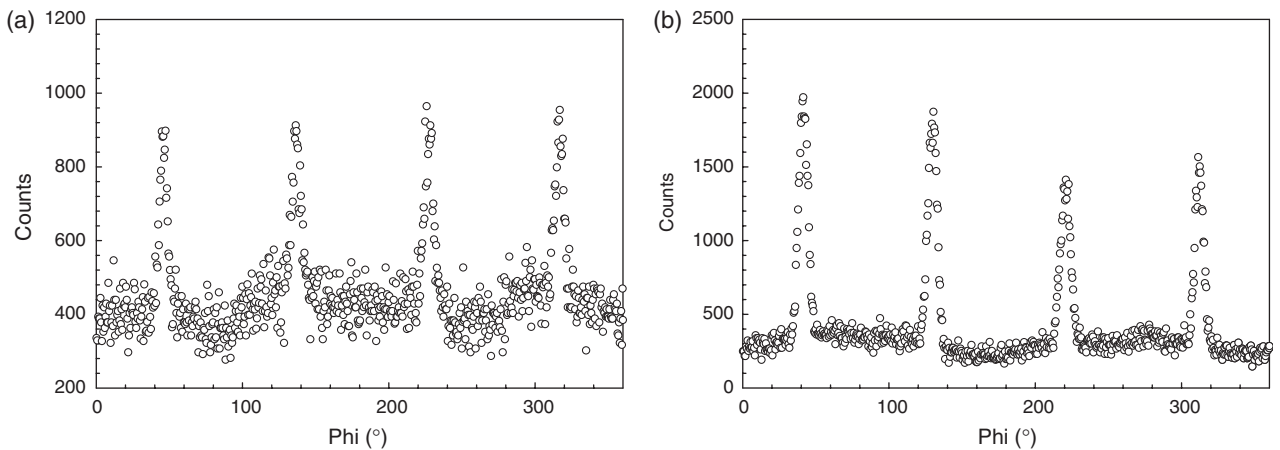
Fig. 4. YBCO (113) ϕ-scans showing the change of in-plane texture with the partial pressure of oxygen (pO_2). Processing condition: (a) 745°C and $pO_2 = 180$ ppm; and (b) 745°C and $pO_2 = 40$ ppm.
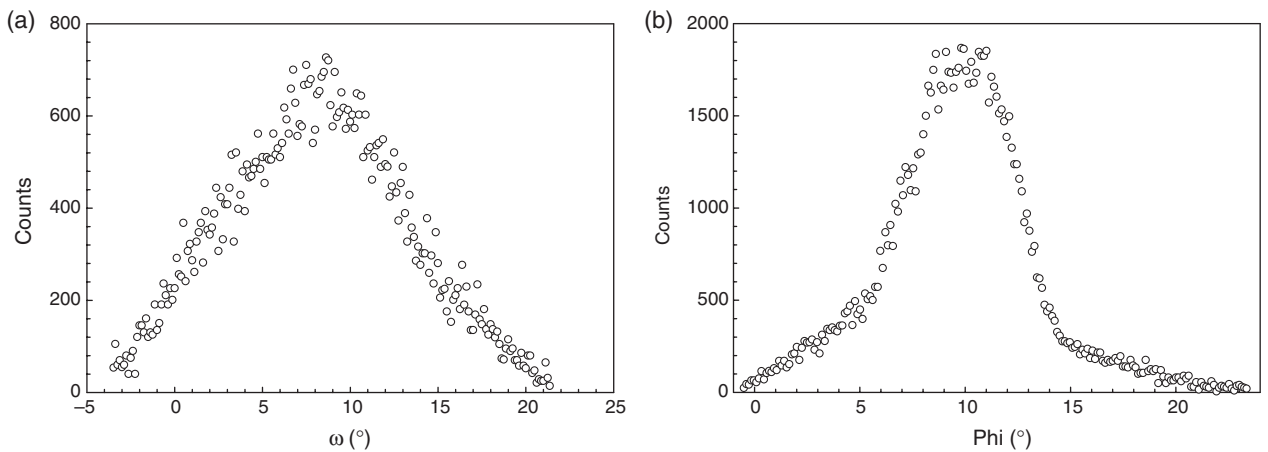

Fig. 5. YBCO (003) ω-scans showing out-of-plane texture change of YBCO on NiW and Ni substrates. Samples were converted at 745°C in a furnace gas of one atmosphere contained (a) 180 ppm oxygen and (b) 40 ppm oxygen.

(r^*) increases with the CeO$_2$ deposition temperature. On the other hand, based on the phase diagram, the driving force for the YBCO formation increases with pO_2. For sample of NW-180, as the CeO$_2$ was deposited at lower temperature of 600°C, so the r^* should be smaller than those deposited at 700°C. Relatively high pO_2 (180 ppm) applied a high driving force for the YBCO formation. As a result, in addition to the interface nu-

cleation, nuclei on relative larger defects such as voids and second phase precipitations prevailed and polycrystalline film was formed. A smaller driving force with low pO_2 should suppress the unwanted random nuclei on defects. Sample NW-40 is just the case with interface nucleation dominating. Because of the low driving force, YBCO grains lost their tracks during the epitaxial growth, ended up half way, and left the upper portion

Fig. 6. YBCO (113) ϕ-scans showing the change of in-plane texture with oxygen partial pressure at 745°C. Samples were converted at (a) $pO_2 = 180$ ppm, and (b) $pO_2 = 40$ ppm.
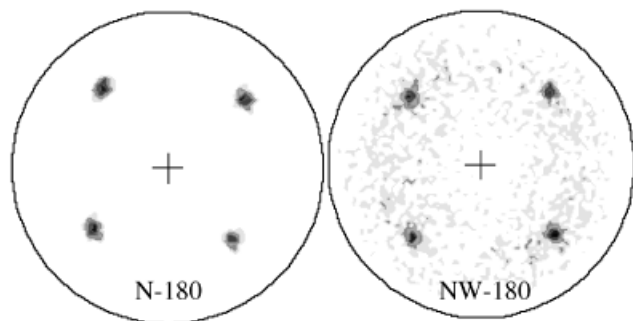
Fig. 7. Linear scale YBCO (113) Pole figures with background sub-contracted (intensity-contour plots) for sample N-180 and NW-180, the four poles indicate *c*-oriented grains with *a*–*b* in-plane alignment. The background noise is reflections of random oriented grains. Compared with sample NW-180, sample N-180 shows strong epitaxial growth and less random grains.

polycrystalline. The low performance of N-40 is because the combination effect of the high energy barrier and low driving force that rendered low nucleation rate and large grains with weak link at grain boundaries.

Figure 9 shows cross-sectional TEM image taken in the vicinity of the interfaces of YBCO/CeO$_2$/YSZ/Y$_2$O$_3$/NiW of sample NW-40. A *c*-axis oriented YBCO layer with in-plane alignments is observed on the CeO$_2$ cap layer, which is a robust layer and can carry high current density. But YBCO grains on the upper portion of the film tends to tilt and form large angle grain boundaries. So the current carrying ability for the upper portion is very limited. This TEM image is in good agreement with the previous analysis. The degradation in the upper

portion of YBCO films, called "dead layer," has also been observed in other approaches, and usually appears in a relatively thick film.[22,28–32] The characteristics of this layer includes the development of misoriented YBCO grains or porosity,[28,33,34] formation of second phases,[29,35,36] oxygen deficiencies, changes in stoichiometry,[37] *a*-axis oriented grains,[38] and other defects. For sample NW-40, if we count out the dead top layer, J_c should be double and comparable to that of sample N-180.

The reason why YBCO grains lost their tracks of epigrowth under small driving force and formed a polycrystalline layer on the upper portion is still unclear. Whereas even at very low pO_2, the compositional change at the growth front and random-oriented nuclei should be responsible for the formation of polycrystalline at the upper portion of the film. The RBS analysis in Fig. 3 does not show observable macroscopic changes in the composition. If the compositional change is one of the reasons for the polycrystalline nucleation, it must be a locally compositional aggregation formed before or during the crystallization. For example, the formation of BaCO$_3$ phase[24] will cause barium aggregations.

Figure 10 shows the J_c measurement of sample N-180 in self-field and in fields up to 0.5 T. The inset is a plot of J_c versus magnetic field. This is the first demonstration of critical current density at 77 K in self-field above 1 MA/cm^2 for a non-fluorine MOD approach. However, its performance in a magnetic field is inferior to those films prepared by PLD or e-beam BaF$_2$ approaches, which generally give a ratio of $J_c(0T)/J_c(0.5\ T) = 4$–5.[39] The high ratio of $J_c(0T)/J_c(0.5\ T)$ in this measurement has a good agreement with the large angle grain boundaries either from the upper dead layer or from the texture of Ni–RABiTS, or both. Because the broad texture of the Ni substrate ($\Delta\omega = 10.3°$, $\Delta\Phi = 10.7°$) and the CeO$_2$ cap layer ($\Delta\omega = 10.1°$, $\Delta\Phi = 10.5°$ 1) weak links exist in the YBCO film.
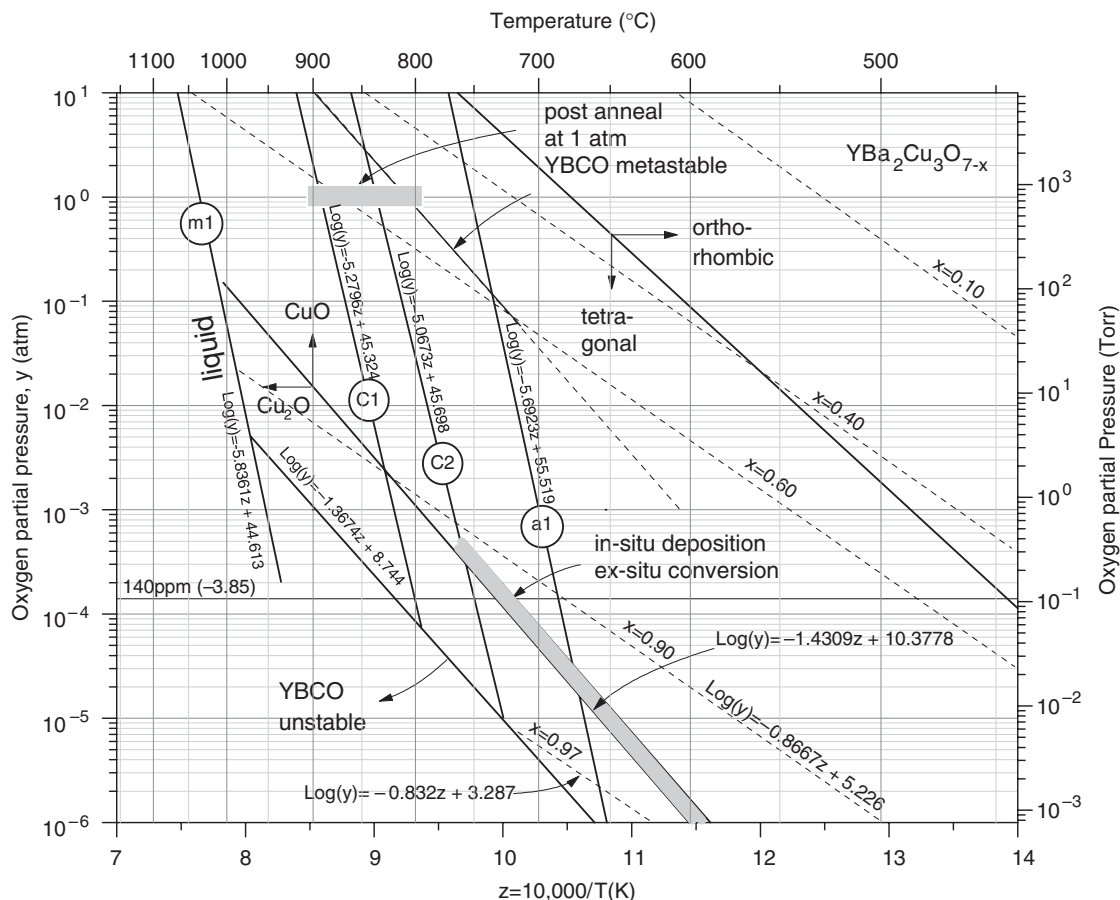
Fig. 8. YBCO phase diagram showing the temperature and oxygen partial pressure dependence of possible phases and orientations. Note: a1: *a*-axis oriented YBCO; c2, *c*-axis oriented YBCO; c1, strongly *c*-axis oriented YBCO; m1, melting line.[26, 27]
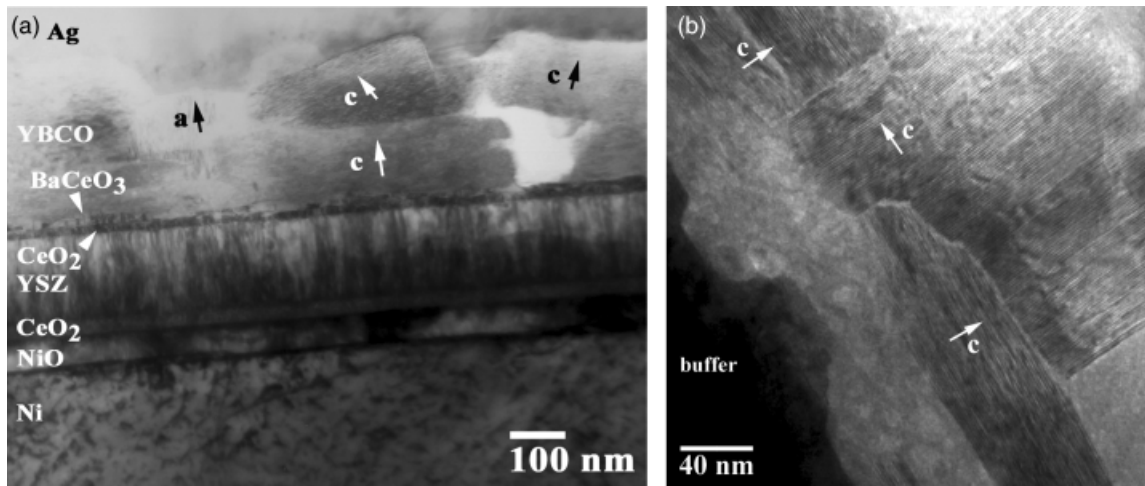
Fig. 9. TEM image taken at the vicinity of the interfaces of YBCO/CeO$_2$/YSZ/Y$_2$O$_3$/Ni of sample NW-40. (a) A reaction layer of BaCeO$_3$ and all other buffer layers are clearly visible. YBCO grains outgrew from the interface and formed *c*-axis oriented texture with *a-b* in-plane alignment. The upper portion shows the feature of polycrystalline films. (b) *a*-axis oriented grains are usually observed at interface.
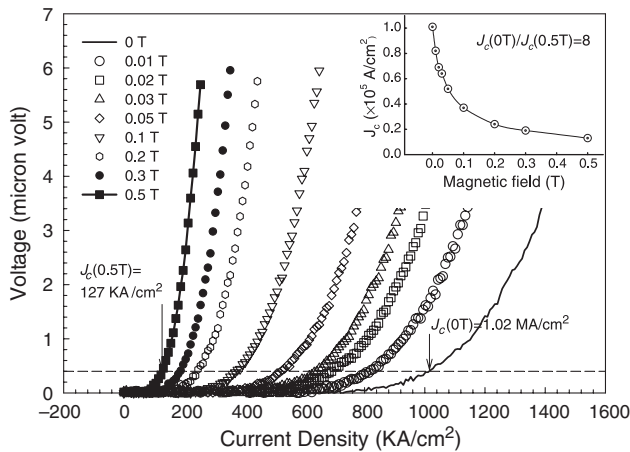
Fig. 10. The magnetic field dependence of current density at 77 K for sample N-180. The high ratio of $J_c(0T)/J_c(0.5\text{ T})$ indicates weak links at YBCO grain boundaries. The in-set plot shows the magnetic field dependence of J_c. The magnetic field, H, was applied parallel to the *c*-axis direction ($H//C_\perp$) and 1 μV/cm was used as the criterion of I_c.

IV. Summary

Superconducting YBCO films with a J_c of 1.02 MA/cm^2 at 77 K were prepared on Ni/CeO$_2$/YSZ/CeO$_2$ substrates. This is the first report of YBCO films on a RABiTS substrate that can carry a critical current density over 1 MA/cm^2 through a fluorine-free MOD approach. Experimental data and analysis show that the deposition temperature of the CeO$_2$ cap layer is one of the key factors that affect the nucleation process in terms of the energy barrier and reactivity. By reducing the pO$_2$ we realized epitaxial growth of Y123 phase on NW series substrates, even though the growth was not that robust and ended up half way in the film. YBCO films with better performance can be expected only when the polycrystalline nucleation is suppressed and the *c*-axis oriented grains from interface nucleation and epitaxial growth dominate. Based on our experiments and data from previous publications, a revised YBCO phase diagram is reported, which will especially fit for the YBCO conversion in the *ex situ* MOD process.

Acknowledgment

REFERENCES

[1]P. Barboux *et al.*, "Bulk and Thick-Films of the Superconducting Phase YBa$_2$Cu$_3$O$_{7-Y}$ Made by Controlled Precipitation and Sol–Gel Processes," *J. Appl. Phys.*, **63** [8] 2725–9 (1988).

[2]A. H. Hamdi *et al.*, "Formation of Thin-Film High-T$_c$ Superconductors by Metalorganic Deposition," *Appl. Phys. Lett.*, **51** [25] 2152–4 (1987).

[3]M. Kawai *et al.*, "Formation of Y–Ba–Cu–O Superconducting Film by a Spray Pyrolysis Method," *Jpn. J. Appl. Phys. Part 2 – Letters*, **26** [10] L1740–2 (1987).

[4]T. Kumagai *et al.*, "Preparation of Superconducting YBa$_2$Cu$_3$O$_{7-Delta}$ Thin-Films by the Dipping-Pyrolysis Process Using Organic-Acid Salts," *Chem. Lett.*, [8] 1645–6 (1987).

[5]C. E. Rice, R. B. Vandover, and G. J. Fisanick, "Preparation of Superconducting Thin-Films of Ba$_2$YCu$_3$O$_7$ by a Novel Spin-on Pyrolysis Technique," *Appl. Phys. Lett.*, **51** [22] 1842–4 (1987).

[6]R. W. Schwartz, "Chemical Solution Deposition of Perovskite Thin Films," *Chem. Mater.*, **9** [11] 2325–40 (1997).

[7]R. W. Schwartz *et al.*, "A Comparison of Diol and Methanol-Based Chemical Solution Deposition Routes for PZT Thin Film Fabrication," *Integr. Ferroelectr.*, **18** [1–4] 275–86 (1997).

[8]F. F. Lange, "Chemical Solution Routes to Single-Crystal Thin Films," *Science*, **273** [5277] 903–9 (1996).

[9]A. Goyal *et al.*, "Strengthened, Biaxially Textured Ni Substrate with Small Alloying Additions for Coated Conductor Applications," *Physica C*, **382** [2–3] 251–62 (2002).

[10]F. Parmigiani *et al.*, "Observation of Carboxylic Groups in the Lattice of Sintered Ba$_2$YCu$_3$O$_{7-Y}$ High-T$_c$ Superconductors," *Phys. Rev. B*, **36** [13] 7148–50 (1987).

[11]A. Gupta *et al.*, "Superconducting Oxide-Films with High Transition-Temperature Prepared from Metal Trifluoroacetate Precursors," *Appl. Phys. Lett.*, **52** [24] 2077–9 (1988).

[12]P. C. McIntyre *et al.*, "Texture Development in Ba$_2$YCu$_3$O$_{7-X}$ Films from Trifluoroacetate Precursors," *J. Mater. Res.*, **5** [12] 2771–9 (1990).

[13]P. C. McIntyre *et al.*, "Effect of Growth-Conditions on the Properties and Morphology of Chemically Derived Epitaxial Thin-Films of Ba$_2$YCu$_3$O$_{7-X}$ on (001) LaAlO$_3$," *J. Appl. Phys.*, **71** [4] 1868–77 (1992).

[14]P. C. McIntyre, M. J. Cima, and A. Roshko, "Epitaxial Nucleation and Growth of Chemically Derived Ba$_2$YCu$_3$O$_{7-X}$ Thin-Films on (001) SrTiO$_3$," *J. Appl. Phys.*, **77** [10] 5263–72 (1995).

[15]J. A. Smith, M. J. Cima, and N. Sonnenberg, "High Critical Current Density Thick MOD-Derived YBCO Films," *IEEE Trans. Appl. Supercond.*, **9** [2] 1531–4 (1999).

[16]Y. Xu, K. Leonard, and A. Goyal, "High Performance YBCO Films by the Hybrid of Non-Fluorine Yttrium and Copper Salts with Ba-TFA," *Physica C*, **421**, 67–72 (2005).

[17]Y. Xu, K. Leonard, and A. Goyal, "Liquid Phase Enhanced Hybrid MOD Approach for High Performance YBCO Films Development," *IEEE*, **15** [2] 2617–9 (2005).

[18]T. Araki, K. Yamagiwa, and I. Hirabayashi, "Fabrication of YBa$_2$Cu$_3$O$_{7-x}$ film by Metalorganic Deposition Method Using Trifluoroacetates and its Process Conditions," *Cryogenics*, **41** [9] 675–81 (2001).

[19]Y. L. Xu *et al.*, "Deposition of Epitaxial YBCO Thin Film on Single Domain YBCO Substrate for the Development of RF Components," *IEEE Trans. Appl. Supercond.*, **11** [1] 2865–8 (2001).

[20]Y. Xu *et al.*, "Fabrication of High J_c YBa$_2$Cu$_3$O$_{7-d}$ Films Using A Fluorine-Free Sol–Gel Approach," *J. Mater. Res.*, **18** [3] 677–81 (2003).

[21]A. Goyal *et al.*, "High Critical Current Density Superconducting Tapes by Epitaxial Deposition of YBa$_2$Cu$_3$O$_x$ Thick Films on Biaxially Textured Metals," *Appl. Phys. Lett.*, **69** [12] 1795–7 (1996).

[22]B. W. Kang *et al.*, "Comparative Study of Thickness Dependence of Critical Current Density of $YBa_2Cu_3O_{7-delta}$ on (100) $SrTiO_3$ and on Rolling-Assisted Biaxially Textured Substrates," *J. Mater. Res.*, **17** [7] 1750–7 (2002).

[23]M. Pernet *et al.*, "Texture Influence on Critical-Current Density of YBCO Films Deposited on (100)-MgO Substrates," *Physica C*, **235**, 627–8 (1994).

[24]Y. Xu, *High J_c Epitaxial $YBa_2Cu_3O_7$- Films Through a Non-Fluorine Approach for Coated Conductor Applications*, in: Chemicals and materials engineering. University of Cincinnati, Cincinnati, 2003.

[25]Y. Xu *et al.*, "Preparation of YBCO Films on CeO_2-Buffered (001) YSZ Substrates by a Non-Fluorine MOD Method," *J. Am. Ceram. Soc.*, **87** [9] 1669–76 (2004).

[26]R. Feenstra *et al.*, "Effect of Oxygen-Pressure on the Synthesis of $YBa_2Cu_3O_{7-X}$ Thin-Films by Postdeposition Annealing," *J. Appl. Phys.*, **69** [9] 6569–85 (1991).

[27]C. P. Poole, *Handbook of Superconductivity*. Academic Press, New York, 2000.

[28]S. R. Foltyn *et al.*, "Relationship Between Film Thickness and the Critical Current of $YBa_2Cu_3O_{7-delta}$-Coated Conductors," *Appl. Phys. Lett.*, **75** [23] 3692–4 (1999).

[29]K. J. Leonard *et al.*, "Microstructural Characterization of Thick $YBa_2Cu_3O_7$-Delta Films on Improved Rolling-Assisted Biaxially Textured Substrates," *J. Mater. Res.*, **18** [7] 1723–32 (2003).

[30]R. Wordenweber, "Growth of High-T-c Thin Films," *Supercond. Sci. Technol.*, **12** [6] R86–102 (1999).

[31]A. I. Usoskin *et al.*, "Growth of HTSC Films with High Critical Currents on Polycrystalline Technical Substrates," *Appl. Supercond*, **148**, 499–502 (1995).

[32]M. S. Hatzistergos *et al.*, "Microstructural and Electrical Characterization of Gas Cluster Ion Beam-Smoothed YBCO Films," *IEEE Trans. Appl. Supercond.*, **13** [2] 2470–3 (2003).

[33]S. Sievers *et al.*, "Grain-Orientation in Thick Laser-Deposited $Y_1Ba_2Cu_3O_{7-Delta}$ Films—Adjustment of C-Axis Orientation," *J. Appl. Phys.*, **78** [9] 5545–8 (1995).

[34]K. J. Leonard *et al.*, "Thickness Dependence of Microstructure and Critical Current Density of $YBa_2Cu_3O_7$-Delta on Rolling-Assisted Biaxially Textured Substrates," *J. Mater. Res.*, **18** [7] 1733 (2003).

[35]K. D. Develos *et al.*, "On the Origin of Surface Outgrowths in Pulsed-Laser-Deposited $YBCO/CeO_2/Al_2O_3$ Thin Films," *Physica C*, **361** [2] 121–9 (2001).

[36]K. Develos *et al.*, "Microstructure of $YBa_2Cu_3O_{7-y}$ Films on CeO_2-Buffered Al_2O_3," *Physica C*, **357**, 1353–7 (2001).

[37]S. R. Foltyn *et al.*, "Influence of Deposition Rate on the Properties of Thick $YBa_2Cu_3O_{7-Delta}$ Films," *J. Mater. Res.*, **12** [11] 2941–6 (1997).

[38]J. Lian *et al.*, "Structural Characterization of Epitaxial YBCO Thin Films Prepared by a Fluorine-Free Sol–Gel Method for Coated Conductors," *Supercond. Sci. Technol.*, **16** [8] 838–4 (2003).

[39]D. P. Norton *et al.*, "Epitaxial $YBa_2Cu_3O_7$ on Biaxially Textured Nickel (001): An Approach to Superconducting Tapes with High Critical Current Density," *Science*, **274** [5288] 755–7 (1996). □